Effect of Annealing Temperature and Time Over the Microstructural, Mechanical and Electrical Properties of Deformed Al Wires (A6)

Lin CHEN [1, 2, 3], Meigui OU [1, 2, 3] *, Yilong LIANG [1, 2, 3], Yu LIANG [1, 2, 3]

[1] *College of Materials and Metallurgy, Guizhou University, Guiyang 550025, China*
[2] *Key Laboratory for Materials Structure and Strength of Guizhou Province, Guiyang 550025, China*
[3] *National Local Co-construction Engineering Laboratory for High Performance Metal Structure Material and Manufacture Technology, Guiyang 550025, China*

http://doi.org/10.5755/j02.ms.37232

Received 15 May 2024; accepted 1 August 2024

Al wires with different deformation were obtained by cold-drawing and annealing treatment. The microstructure, mechanical, and electrical properties of the wires annealed at different temperatures and times were studied using SEM, universal testing machine, and DC resistance tester. The results indicate that as the annealing temperature and time increase, the UTS of Al decreases, while the EL and EC increase simultaneously. During the annealing procedure, recrystallization is observed to begin at 300 ℃ and complete at 350 ℃. Compared with the beginning of recrystallization, the recrystallized grain diameter increases from 11.34 μm to 20.59 μm, while the UTS decreases by 24.1 %, the EL increases by 74 %, and the EC increases by 3 %. When annealed at 315 ℃ for 1h, the recrystallization begins in the samples with 90 % deformation, and completes when the annealing time is increased to 4.5 h, the grain diameter increases from 7.67 μm to 20.71 μm; though the tensile decreases by 24.3 %, the EL and EC increase by 97.5 % and 2.8 %, respectively.

Keywords: aluminum wires, annealing treatment, recrystallization, mechanical properties, electric conductivity.

1. INTRODUCTION

Cables play an essential role in the electrical system, facilitating power transmission [1 – 4]. The cable is composed of a metal core and an outer insulating material, and it could be said that the performance of the metal core largely determines the quality of the cable [5, 6]. In the early days of long-distance power transmission, copper was the material of choice for the metal wire core due to its excellent EC and mechanical properties [7 – 9]. However, the high density of copper does present a challenge in terms of span spacing, which can be a limiting factor in the cost-effectiveness of long-distance power transmission. This could potentially impact the sustainability of the cable industry. While Al has a lower EC than copper, it is worth noting that its ratio of EC to weight is twice that of copper. In addition, the specific strength of Al is 30 % higher than that of copper, and the flexibility and corrosion resistance are also better than that of copper [10 – 14]. Therefore, the wide application of Al wire in the power industry can greatly reduce the cost of power transmission. "replacing copper with aluminum" has become a new development trend, which is an inevitable requirement to promote the high-quality development of the cable industry [15].

To date, a large number of scholars have carried out research on Al wires, including studies on their EC, EL, UTS, YS, fatigue strength, friction properties, etc. It has been shown that elastic and microplastic deformation features are characteristic of the wire as a whole, and that they are very sensitive to changes in microstructure and correlate with the results of diffraction methods, showing complex structural changes [16]. A new experimental test bench intended to perform fretting fatigue tests on individual strands of overhead conductors is used to study the wire-to-clamp and the wire-to-wire contact configurations [17]. The variety of the material's hardened states significantly affected its fatigue strength [18]. Moreover, Pan et al. concluded that the ultimate tensile and yield strength increases significantly with increasing Fe content, while the conductivity decreases slightly. In addition, in high Fe-containing alloys, the volume fraction of fine intermetallic particles is larger and the subgrain size is smaller, resulting in a much higher creep resistance. As the Fe content increases from 0.3 to 0.7 %, the creep threshold stress increases from 24.6 MPa to 33.9 MPa, respectively. The true stress exponent values of the three experimental alloys are close to 3, indicating that the creep mechanisms of the 8xxx alloys are all dislocation-controlled [19]. Hou et al. artificially aged 6201RE Al alloy conductors to obtain a large number of dispersed nanoscale precipitated phases. The precipitation of alloying elements in the form of nano-precipitated phases plays a strengthening role, reduces the concentration of alloying elements in the matrix, and reduces the lattice distortion, resulting in the 6201RE Al alloy obtaining both high strength (352.3 MPa) and high EC (56.0 % IACS). Likewise, nanoscale precipitates in Al alloys can improve the strength and EC of Al alloys [20]. Luo et al. explored and found that the cold-drawing process greatly increases the YS of commercially pure Al wire while maintaining resistivity. The increase in strength of cold-drawn Al wire is mainly due to GB and dislocation

* Corresponding author. Tel.: +86-18984584582.
E-mail: *mgou1@gzu.edu.cn* (M. OU)

strengthening. Texture reinforcement works at higher strains.GB and dislocation scattering are the main reasons for the decrease in conductivity [21]. Some scholars have also studied the effect of annealing treatment on the microstructure and properties of pure aluminum wire, and the results showed that the texture evolution, the dislocation recovery and the subgrain growth during the recrystallization should be responsible for the strength degradation of commercially pure Al wires annealed at different temperature and time [22]. During the ultrafast annealing process, the grain diameters of pure aluminum increase from 2.05 μm to 17.10 μm with the increase of annealing temperature from 410 ℃ to 520 ℃, the UTS decreases from 116.48 MPa to 53.43 MPa, and the uniform EL increases from 1.20 % to 39.78 % [23]. Table 1 shows the summarized comparisons of the above studies on Al conductors.

The above studies have indicated that the multipass drawing process during the production of Al wires may potentially result in the formation of a significant number of piling dislocations within the microstructure. This could lead to an enhancement in the UTS of Al wires, while simultaneously reducing the EC and EL. It would seem necessary, therefore, to subject the deformed Al wires to an annealing treatment, to alleviate the severe work hardening [24, 25]. Annealing parameters play a key role in the microstructure and mechanical properties of pure Al materials. However, there is still a lack of studies focusing on the effect of the microstructure during the annealing process on the mechanical and electrical properties of deformed pure Al wires. In this paper, we aim to shed light on the relationship between annealing treatment parameters (temperature and time), the corresponding microstructure and comprehensive properties of deformed pure Al wire. Our findings could potentially serve as a theoretical and experimental foundation for the production of Al wires with enhanced comprehensive properties, thereby expanding their applications in the power industry.

2. MATERIALS AND METHODS

The experimental raw materials were A6 Al rods with a diameter of 9.5 mm, and the chemical composition is shown in Table 2.

The samples with different deformation (50 % and 90 %) were obtained by multi-pass cold-drawing of Φ 9.5 mm Al wires by wire drawing machine and annealed by box-type resistance furnace. Annealing parameters are shown in Table 3.

Table 2. Chemical composition of A6 Al wires (wt.%)

Fe	Si	Cu	Cr	V	Cr	Al
0.18	0.058	0.0047	0.01	0.00033	0.0001	balance

The metallographic samples were polished using 800 ~ 7000# SiC sandpaper and then electrolytic polished by electrolytic polishing etch meter (EP-06X) for 30 s at 0 ℃. The etching solution contained perchloric acid (10 V.%) and alcohol (90 V.%), and the etching voltage was 25 V. Subsequently, the samples were anodic coated in fluoroboric acid solution at the voltage of 20 V for 45 s [26, 27]. The microstructure of samples was observed by a polarizing microscope (OLYMPUS GX 71) and scanning electron microscope (ZEISS SUPRA 40), respectively. EBSD technique was used to analyze the percentage of LAGB and the local orientation difference of the samples, etc. Image-Pro Plu s6.0 software was used to measure the recrystallization grain size of the sample and calculate the area occupied. The degree of recrystallisation is calculated in accordance with the Eq. 1:

$$D_R = \frac{S_R}{S_A}, \quad (1)$$

where D_R is the degree of recrystallization; S_A is all the areas measured, m; S_R is the area of the region occupied by the recrystallized grains.

The universal testing machine (MTS810) was used to test the UTS and EL of Al wires at different annealing temperatures, and the tensile axis was parallel to the axial direction of the Al wires. Each tensile test value was the average value of 3 samples. The PC36C DC resistance tester was applied to test the electrical resistance of the samples (200 mm in length) in different annealing processes. In order to ensure the accuracy of the results, the room temperature was adjusted to about 18 ℃ by the air conditioner during the measuring process.

Table 1. Summarized comparisons of the studies on Al wires

Material	Technology	Testing properties	Reference
Al wires (without a steel core)	–	Elastic and microplastic	[16]
Overhead line Al conductors	–	Friction properties	[17]
Al wires used for ACSR cables	Drawing	Fatigue strength	[18]
8xxx Al alloys	Fe element addition	UTS, YS, EC and creep	[19]
6201RE Al alloy conductor	Solid-solution strengthening	UTS and EC	[20]
Pure Al rods	Cold drawing	YS, EL and EC	[21]
Commercially pure Al conductor	Annealing treatment	UTS and YS	[22]
Commercial pure Al	Ultra-fast annealing	UTS and EL	[23]
Al wires (A6)	Annealing	UTS, EL and EC	This study

Table 3. Annealing parameters of samples with different deformation

50 % deformation (1 h)	Temperature, ℃								
	300		315		335		350		400
90 % deformation (315 ℃)	Time, h								
	1	1.5	2	2.5	3	3.5	4	4.5	5

The EC of the samples was calculated by the Eq. 2:

$$W = \frac{L}{R \times S \times 5.8 \times 10^7} \times 100\%, \quad (2)$$

where W is the EC %IACS; L is the measured length, m; R is the electrical resistance, Ω; S is the radial section area of the wires, m^2 [28].

3. RESULTS AND DISCUSSION

3.1. Influence of annealing temperature on the microstructure and properties of Al wires

Fig. 1 shows the metallographic microstructure of Al wires with 50% deformation annealed at different temperature for 1 h. It can be observed from Fig. 1 a that the microstructure of cold-drawn samples is typically fibrous, and with the increase of annealing temperature, the fibrous structure gradually changes into the equiaxed recrystallized grains. When the annealing temperature is 300 ℃ (Fig. 1 b), the sample begins to recrystallize, and the diameter of the recrystallization grain is 11.34 μm (Table 4). However, the degree of recrystallization at this stage was very low, and the equiaxed grains are accounted for only about 3 % (in volume). When the temperature is 315 ℃, the recrystallization grains with an average diameter of 11.86 μm increase significantly (Fig. 1 c), and the recrystallization degree reaches about 40 %. At an annealing temperature 335 ℃, the microstructure is dominated by equiaxed grains of 11.93 μm (Fig. 1 d and the recrystallization degree reaches 75 %. When it can be clearly seen that the fibrous structure in the sample annealed at 350 ℃ completely disappears (Fig. 1 e), and the recrystallization is completed, with the average grain diameter of 20.59 μm. The recrystallized grains grow up to 28.62 μm at 400 ℃ (Fig. 1 f), and the grain diameter increases by 39 %, compared with that when recrystallization is just completed (Fig. 1 e). Moreover, the GB becomes flatter and the microstructure uniformity is improved [29 – 31].

Table 4. Recrystallization data of Al wires at different annealing temperatures

Temperature, ℃	D_R, %	Grain diameter, μm
0	0	–
300	3	11.34
315	40	11.86
335	75	11.93
350	100	20.59
400	100	28.62

In order to further analyze the recrystallized microstructure of deformed Al wires annealed at different temperatures, the samples annealed at 315 ℃, 350 ℃ and 400 ℃ were selected for EBSD characterization, and the results are presented in Fig. 2. Fig. 2 a – c) show the IPF of the annealed samples, which are consistent with those in Fig. 1. When the annealing temperature is 315 ℃, recrystallization is not completed, and a large number of fibrous grains exist in the sample. At 350 ℃, the fibrous grains completely disappear, and the recrystallization is completed., and the recrystallized grains further grow up at 400 ℃. Fig. 2 d – f) show the corresponding GB of the samples, and the green and red lines denote the LAGB (misorientation angle in the range of 2° – 15°) and the HAGB (misorientation angle exceeding 15°), respectively. The corresponding GB distribution values are shown in Fig. 2 g – i), in which the percentage of LAGB is calculated according to the Eq. 3:

$$V_{LAGB} = \frac{N_{LAGB}}{N_{HAGB} + N_{LAGB}}, \quad (3)$$

where V_{LAGB} is the percentage of LAGB; N_{LAGB} is the sum of LAGB number, N_{HAGB} is the sum of HAGB number. The formation and aggregation of LAGB are mainly caused by grain deformation and dislocation movement. With the increase of deformation, the newly generated dislocations move to the GB and accumulate into dislocation clusters at the GB due to the blocking effect, increasing the dislocation density near the GB.

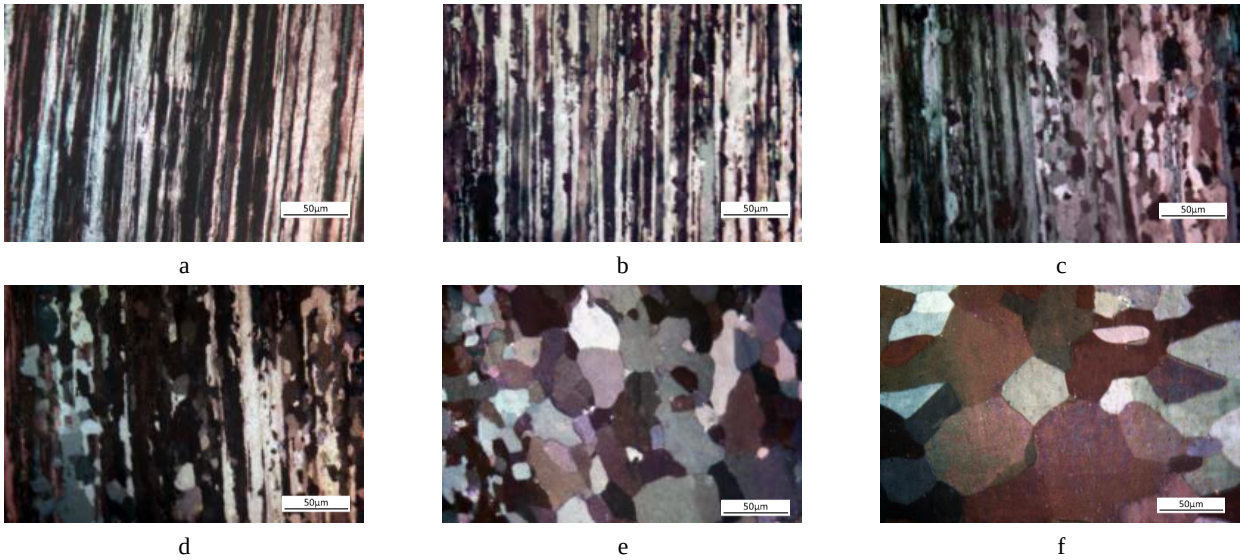

Fig. 1. Metallographic microstructure of Al wires at different annealing temperatures: a – 0 ℃; b – 300 ℃; c – 315 ℃; d – 335 ℃; e – 350 ℃; f – 400 ℃

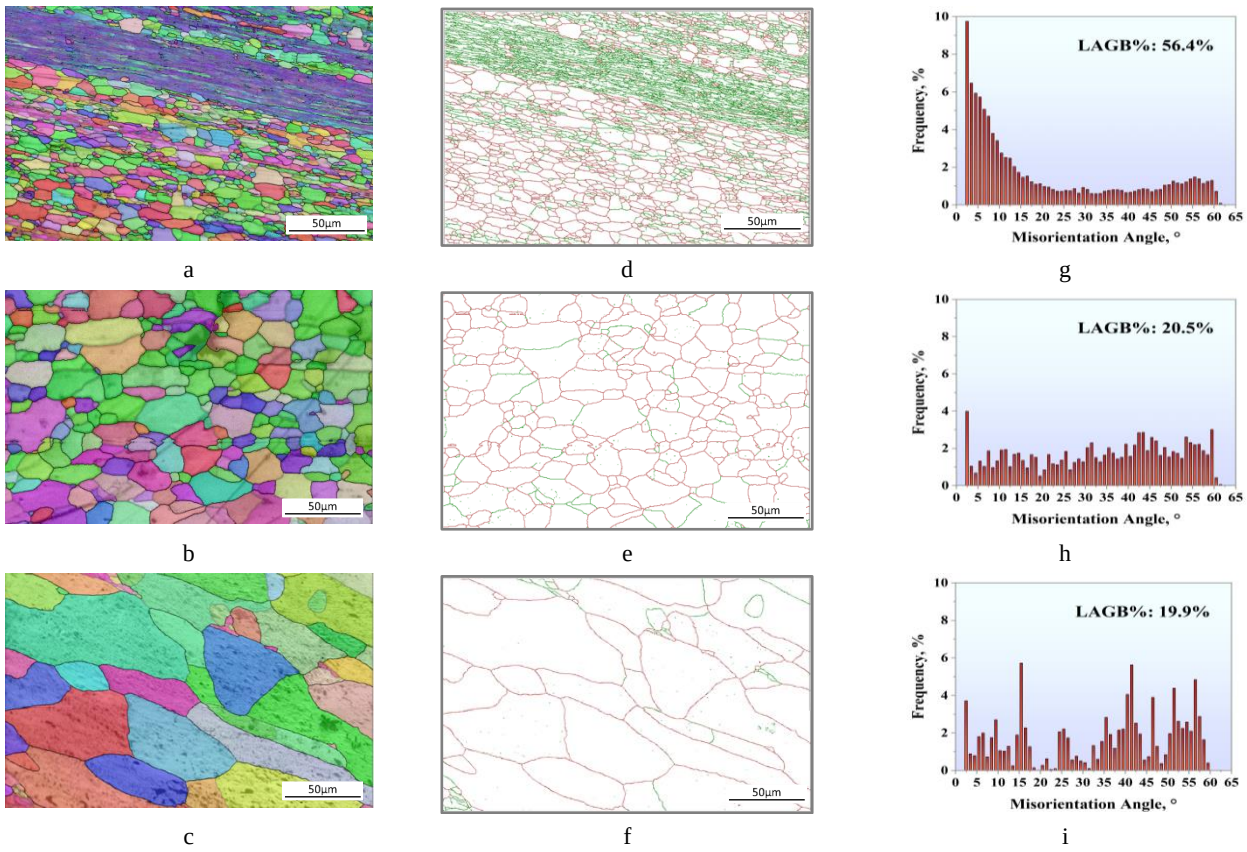

Fig. 2. EBSD characterization of annealed samples: a – 315 ℃; b – 350 ℃; c – 400 ℃; d, e, f – GB images; g, h, i – corresponding GB number distribution

When the dislocation density at the GB continues to increase to a certain extent, dislocation cells will form, and eventually develop into LAGB. In addition, the formation of dislocation groups near the GB and the increase of dislocation density will hinder the further movement of the dislocations and prevent the further plastic deformation of the grains, resulting in the macroscopic work hardening phenomenon [32]. It can be seen from Fig. 2 g – i that with the increase of annealing temperature, the percentage of LAGB decreases from 56.4 % to 19.9 %, indicating that the dislocation density gradually decreases, the stored distortion energy decreases, and the scattering ability of electrons decreases, which will lead to the increasing EL and EC and the decreasing UTS [33].

Fig. 3 a – c show the KAM distribution of the selected samples, which represents the local orientation difference induced by geometric necessary dislocation. The surface stress level of the samples can be reflected through the color contrast, and the local strain is weakened with the color changing from green to blue. It can be found that as the annealing temperature increases, the green areas decrease, and the KAM value decreases from 0.56° to 0.42° (Fig. 3 d – f). The GND density can be calculated by Eq. 4:

$$\rho_{GND} = \frac{2KAM}{\mu b}, \quad (4)$$

where μ is the chosen step size for the EBSD experiment and b is the length of the Burger's vector [34, 35]. It can be calculated that GND density decreases from $3.44 \times 10^{14}/m^2$ to $2.56 \times 10^{14}/m^2$, as the annealing temperature increase from 315 ℃ to 400 ℃. This indicates that the local strain of the deformed samples after the recrystallization and the dislocations near GB decrease during the annealing of increasing temperature.

Fig. 4 shows the SF distribution of the samples. The plastic deformation of the materials is mainly accomplished by sliding. The higher the value of SF is, the higher the probability of sliding systems being activated, and the stronger the plastic deformation ability is. The redder the color of the figures is, the closer the Schmidt factor is to the maximum value of 0.5, and the better the plasticity of the material is [18]. It can be seen in Fig. 4 a and d that the red area is small and not continuous for the sample annealed at 315 ℃, and the SF values are mainly distributed between 0.3 and 0.35. In the case of 350 ℃ (Fig. 4 b and e), the red areas increases and the SF value of more areas is above 0.45. the red region area increases significantly when the temperature reaches 400 ℃ (Fig. 4 c and f), the red region is more continuously distributed, and SF values of many regions are close to 0.5, nearly without SF values below 0.35. This further indicates that the annealed sample at 400 ℃ has the minimum local strain, and the increase of annealing temperature can reduce the local stress and strain, and improve the plasticity of the deformed samples [36 – 38].

Fig. 5 a presents the UTS and EL of the samples at different annealing temperatures. It can be observed that the UTS gradually decreases with the increase of annealing temperature. When recrystallization is completed at 350 ℃, the UTS of the drawn sample changes from 136.47 MPa to 77.7 MPa and decreases by 43 %.

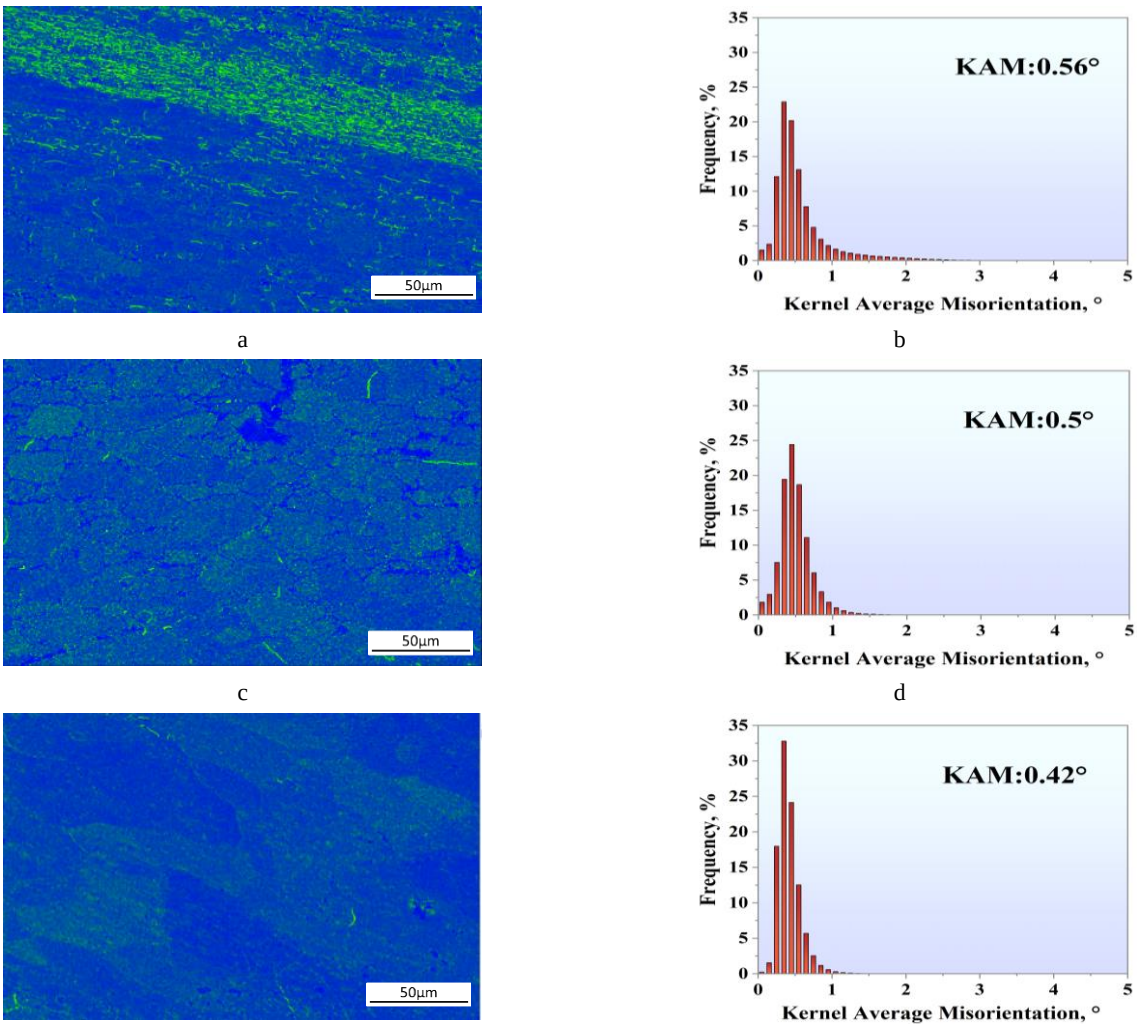

Fig. 3. KAM of annealed samples: a – 315 °C; b – 350 °C; c – 400 °C; d, e, f – corresponding KAM value distribution

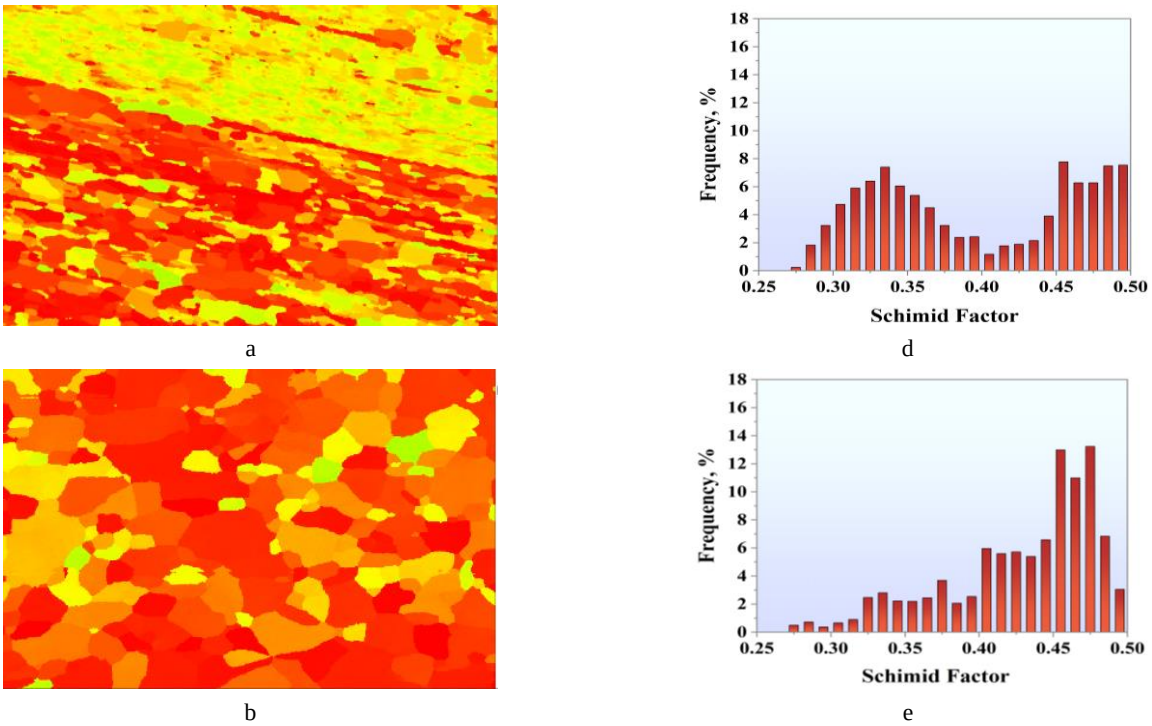

continued on next page

c

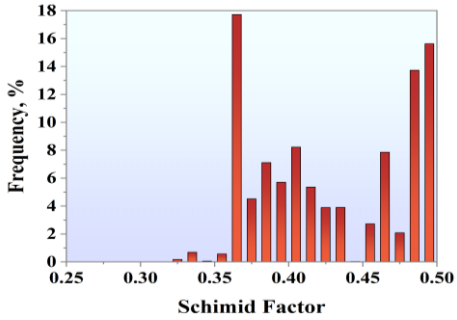

f

Fig. 4. SF distribution of annealed samples: a – 315 ℃; b – 350 ℃; c – 400 ℃; d, e, f – corresponding SF value distribution

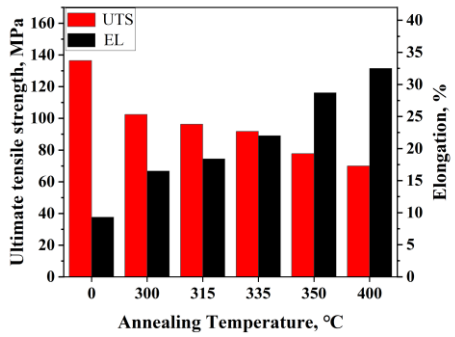

a

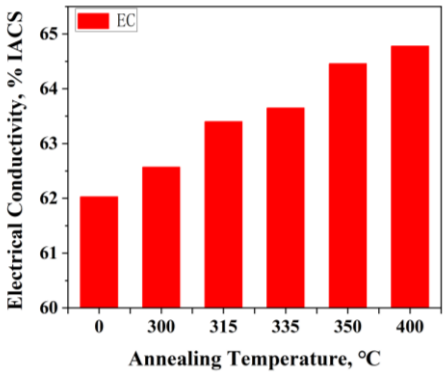

b

Fig. 5. a – UTS, EL; b – EL of the samples at different annealing temperature

When the grain growth occurs at 400 ℃, the UTS further decreases by 49 % to 69.93 MPa, compared with the drawn sample. The variation trend of EL is opposite to the UTS. The EL of the drawn samples and the recrystallized sample is 9.4 % and 28.7 % (350 ℃), respectively (increase by 2 times). After annealing at 400 ℃, the EL of the sample reaches 32.5 % and is 3.5 times that of drawn sample. During the cold-drawing process, the slip occurs inside the grain. With the increase of deform degree, the grain elongates along the deformation direction and the fibrous structure forms (Fig. 1 a), which is unstable due to grain breakage and a large increase in vacancies and dislocations [39]. With the annealing temperature increase from 315 ℃ to 350 ℃, the fibrous structure is gradually replaced by the equiaxed recrystallization structure, and the fibrous structure completely disappears at 350 ℃ (Fig. 1 c), with the percentage of LAGB varied from 56.4 % to 20.5 % and KAM value from 0.56° to 0.5°. When the annealing temperature rises to 400 ℃, the percentage of LAGB and KAM value decreases to 19.9 % (Fig. 2) and 0.42° (Fig. 3), respectively, indicating that the increasing annealing temperature reduces the internal stress, the crystal defects and the storage energy generated during the drawing process. The unstable structure transforms into a stable structure, and the degree of work hardening relieves, finally leading to the decrease of UTS and the increase of EL.

Fig. 5 b shows the EC of the samples at different annealing temperature. As the annealing temperature increase, the EC of the samples gradually increases. Compared with that (62.03 % IACS) of the drawn sample, the EC of the completely recrystallized sample at 350 ℃ (64.46 % IACS) and 400 ℃ (64.78 % IACS) increases by 3.9 % and 4.4 %, respectively. According to the Matthiessen rule, the total resistivity of a metal material can be expressed as: $\rho = \rho_T + \rho_R$, wherein ρ_T is the temperature-dependent resistivity and ρ_R is the resistivity closely related to defect, such as vacancies and dislocations, etc. In the cold-drawing process of Al wires, the defects will be produced, resulting in the scattering of propagating electron waves and reducing the EC [40]. With the increase of annealing temperature, the percentage of LAGB and KAM value decrease from 56.4 % to 19.9 % (Fig. 2) and from 0.56° to 0.42° (Fig. 3), respectively, indicating that the internal stress and the crystal defects are gradually reduced. Therefore, the electron scattering decreases and the EC of the samples is enhanced.

Fig. 6 displays the fracture morphologies of the samples with different annealing temperatures. Ductile dimples exist in a large number of areas on the tensile fracture of the samples before and after annealing, indicating that the fracture mode is a plastic fracture. The size and depth of the dimple are attributed to the plastic deformation ability of the matrix and the number and distribution of the second phase. The stronger the plastic deformation ability of the matrix, the smaller and the more evenly distributed the secondary phase is, the larger and deeper the dimples on the fracture are. On the contrary, the higher the degree of work hardening is, the shallower the dimples are. The fracture dimples of the drawn sample (Fig. 6 a) are small and shallow, and the size is obviously smaller than that of the annealed ones (Fig. 6 b – f)). With the increase of annealing temperature, the dimples' size and depth increase, further manifesting the enhancement of the plasticity of the samples [14, 41].

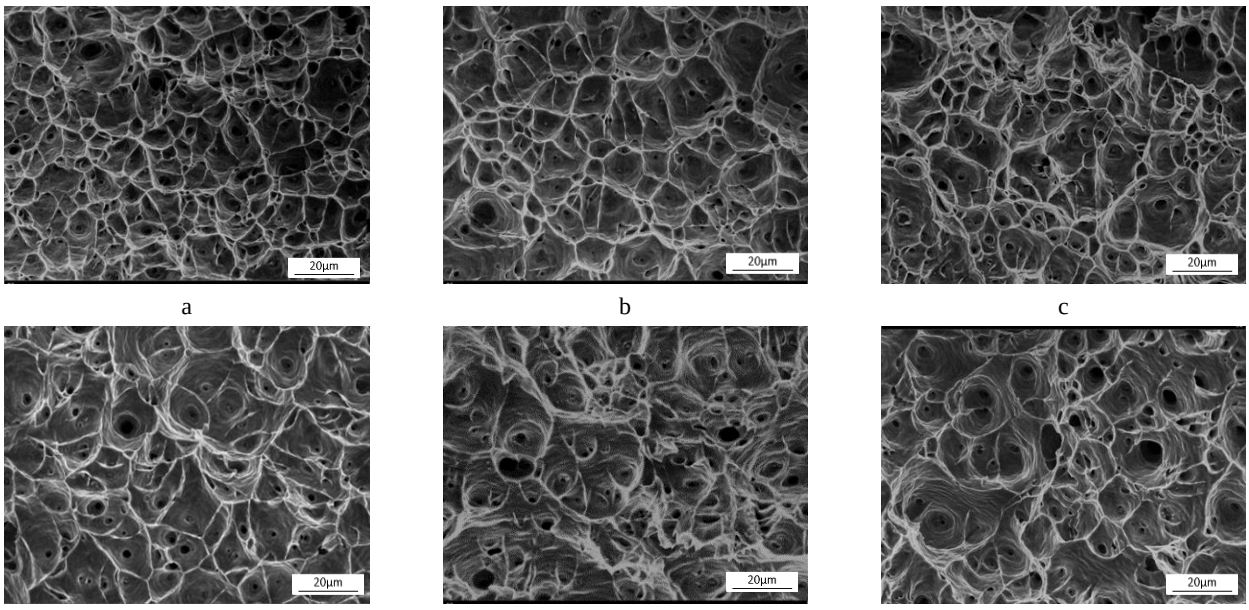

Fig. 6. Fracture morphologies of the samples annealed at different temperatures: a – 0 °C; b – 300 °C; c – 315 °C; d – 335 °C; e – 350 °C; f – 400 °C

3.2. Influence of annealing time on microstructure and properties of deformed Al wires

Fig. 7 shows the metallographic microstructure of Al wires with 90 % deformation annealed at 315 °C for different times. It can be observed that the fibrous structure gradually changes into the equiaxed recrystallized grains with the increase of annealing time. When the annealing time is 1 h (Fig. 7 a), though the sample begins to recrystallize, the microstructure is dominated by fibrous grains, and the equiaxed grains in diameter 7.67 μm (Table 5) are accounted for only about 5 % (in volume). When the fibrous structure in the sample annealed at 4.5 h completely disappears (Fig. 7 h), the recrystallization is basically completed, with an average grain diameter of 20.71 μm. At an annealing time 5 h (Fig. 7 i), the recrystallized grains grow up to 24.7 μm, and the grain diameter increases by 19 % compared with the sample annealed at 4.5 h.

Table 5. Recrystallization data of the samples at different annealing times

Time, h	D_R, %	Grain diameter, μm
1	5	7.67
1.5	35	10.25
2	53	13.8
2.5	60	14.57
3	75	16.17
3.5	85	16.67
4	92	20.26
4.5	100	20.71
5	100	24.7

The samples annealed for 1 h, 3 h and 5 h were selected for EBSD characterization, and the results are shown in Fig. 8. Fig. 8 a – c) show the IPF images of the annealed sample, which is consistent with the results in Fig. 7. When the annealing time is 1h, the sample begins to recrystallize. After annealing for 3 h, a large number of equiaxed grains are produced in the sample. The recrystallization is completed when the annealing time reaches 5 h. Fig. 8 d – f and Fig. 8 g – i) show the corresponding GB distribution and their number percentages, respectively. According to the calculation by Eq. 1, with the increase of annealing time, the percentage of LAGB decreases from 66.5 % to 52.3 %, indicating that the dislocation density and the stored distortion energy gradually decreases, leading to the decreasing degree of electrons scattering.

Fig. 9 a – c and d – f present the KAM and its value distribution of the samples, respectively. As the annealing time increase from 1 h to 5 h, the KAM value decreases from 0.83° to 0.47°. According to Eq. 2, when the annealing time is 1 h, 3 h and 5 h, the GND density of the samples is respectively $5.05 \times 1014/m^2$, $3.57 \times 1014/m^2$ and $2.87 \times 1014/m^2$, indicating that increasing the annealing time can also reduce the dislocation near the GB after recrystallization and the local strain of the samples.

Fig. 10 shows the SF distribution of the samples, and it can be observed that when the annealing time is 1h, there are fewer red areas, and the SF value is mainly distributed between 0.35 and 0.4 (Fig. 10 a and d). When the annealing time is 3 h, the red region area increases significantly (Fig. 10 b and e). The red area in (Fig. 10 c and f) for the sample annealed for 5 h increases and the distribution is uniform, and most of the SF values are above 0.4. Therefore, increasing the annealing time can further reduce the local stress and strain of the deformed samples, thus improving the plasticity of the material.

Fig. 11 a displays the mechanical properties of deformed samples annealed at different time. It can be observed that the UTS gradually decreases and the EL increases with the increase of annealing time. From the beginning of recrystallization (1 h) to be completed (5 h), the UTS of the sample changes from 108.69 MPa to 82.23 MPa and decreases by 24.3 %.

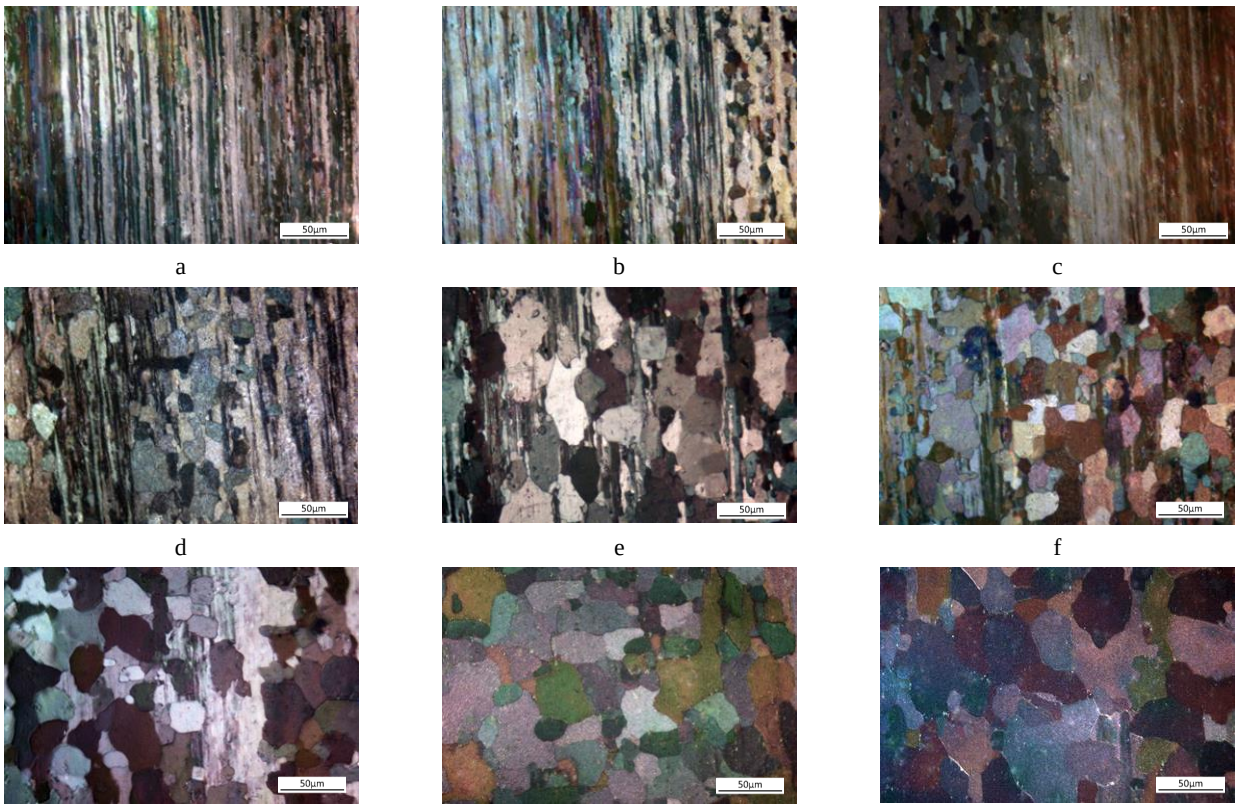

Fig. 7. Metallographic microstructure of the samples at different annealing time: a – 1 h; b – 1.5 h; c – 2 h; d – 2.5 h; e – 3 h; f – 3.5 h; g – 4 h; h – 4.5 h; i – 5 h

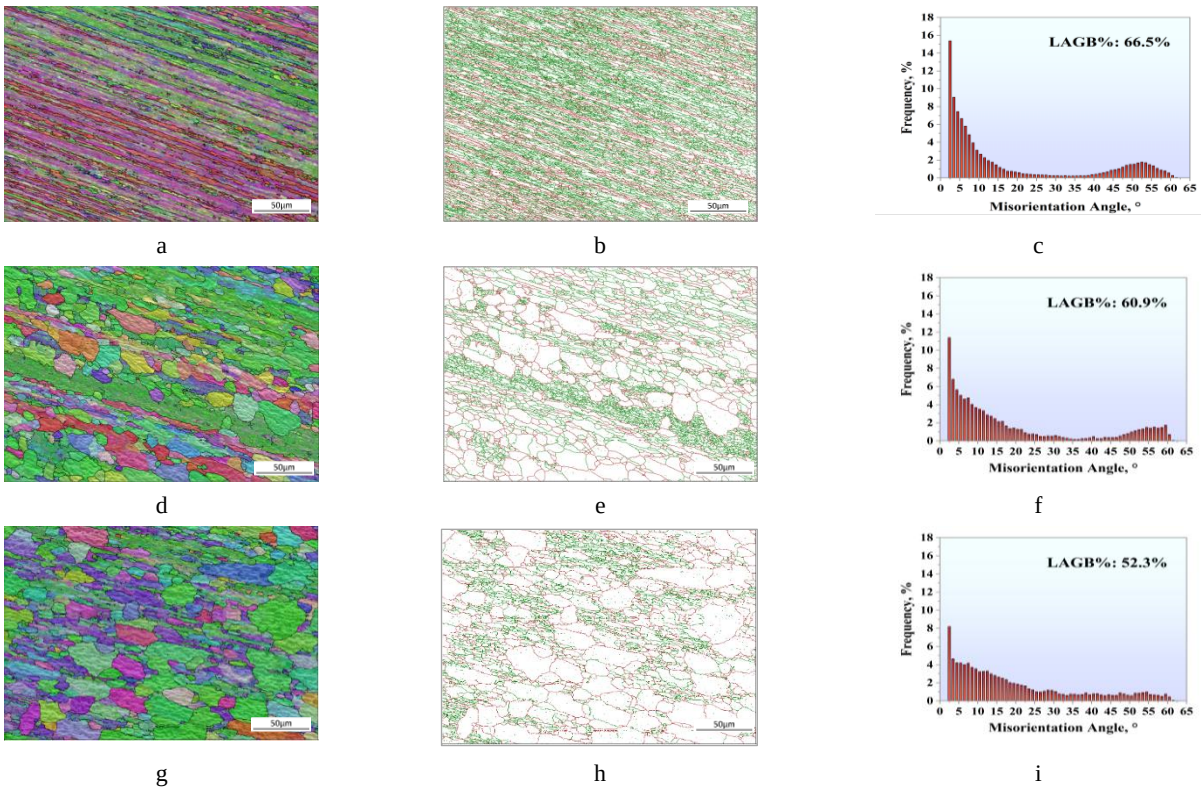

Fig. 8. EBSD characterization of annealed samples: a – 1 h; b – 3 h; c – 5 h; d, e, f – GB maps; g, h, i – corresponding GB value distribution

The EL of the sample increases by 1 time from 14.16 % to 28.24 %, respectively. With the annealing time increase from 1 h to 5 h, the percentage of LAGB varies from 66.5 % to 52.3 % (Fig. 8) and KAM value from 0.83° to 0.47° (Fig. 9), indicating that the increasing annealing time reduces the internal stress, the crystal defects and the storage energy generated during the drawing process.

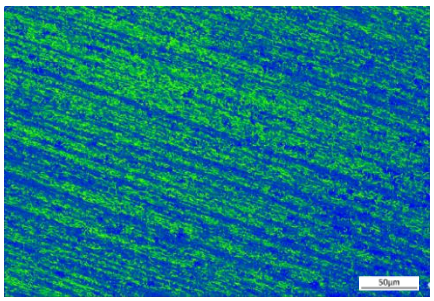

a

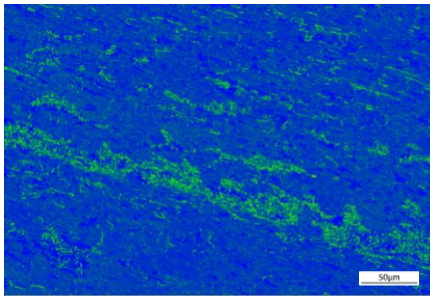

b

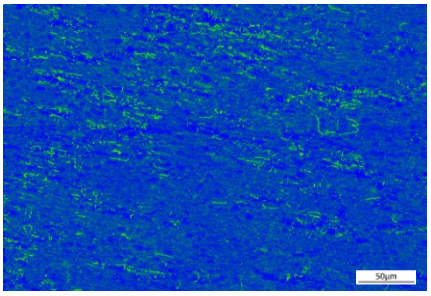

c

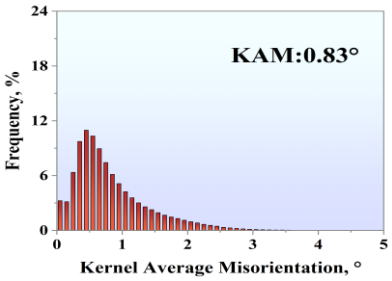

d

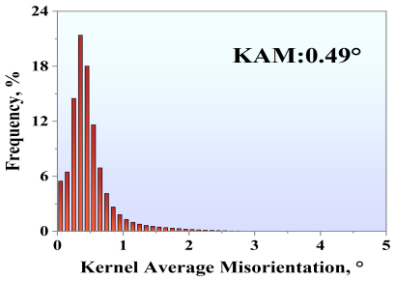

e

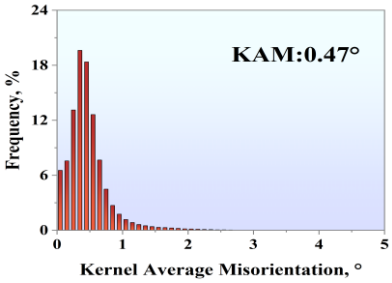

f

Fig. 9. KAM distribution of annealed samples: a – 1 h; b – 3 h; c – 5 h; d, e, f – corresponding KAM value distribution

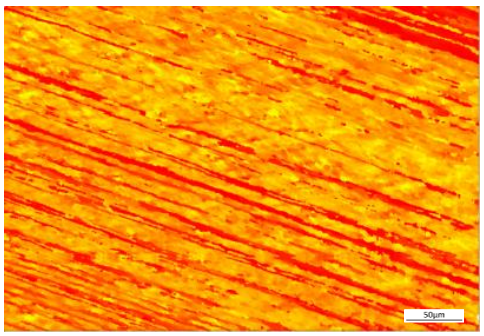

a

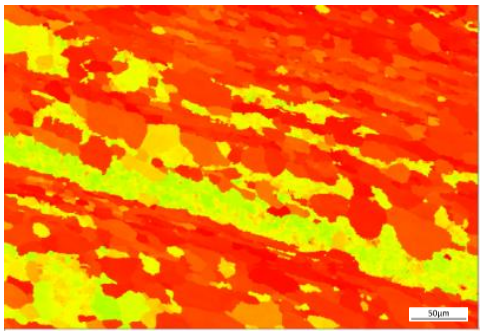

b

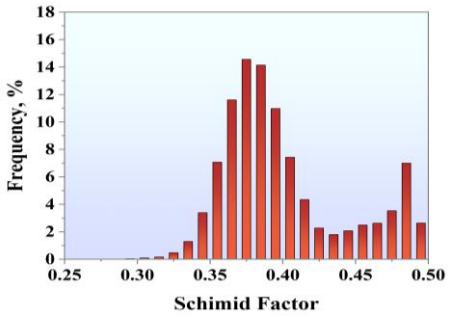

d

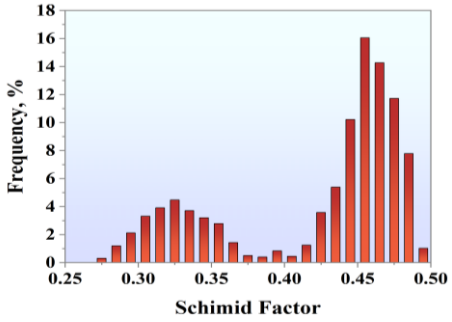

e

continued on next page

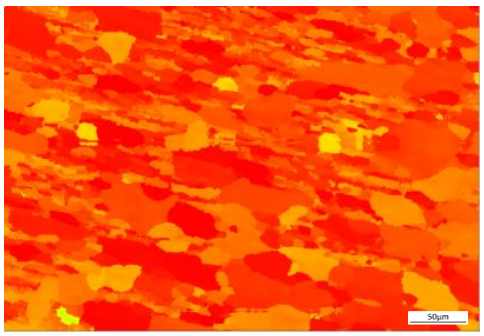

c

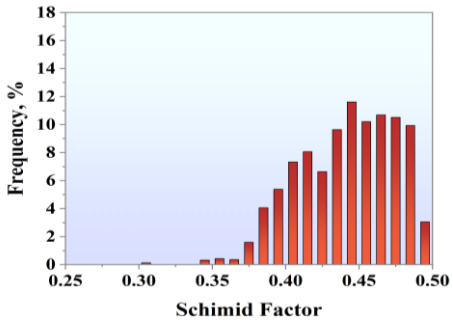

f

Fig. 10. SF distribution of annealed samples: a – 1 h; b – 3 h; c – 5 h; d, e, f – corresponding SF value distribution

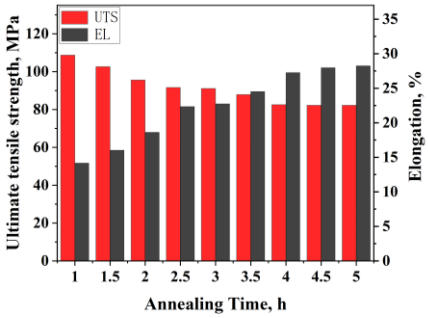

a

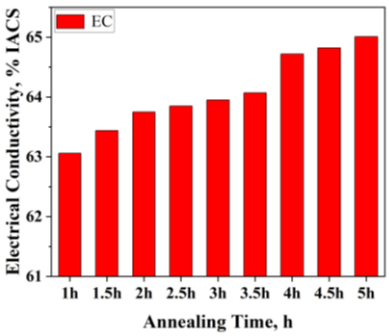

b

Fig. 11. a – mechanical properties; b – EC of the samples annealed for different times

The unstable structure transforms into a stable structure, and the degree of work hardening relieves, finally leading to the decrease of UTS and the increase of EL.

Fig. 11 b shows the EC of the samples annealed at different times. As the annealing time increases, the EC of the samples gradually increases. Compared with that (63.06 % IACS) of the initial recrystallization sample (1 h), the EC of the completely recrystallized sample at 5 h (65.01 % IACS) increases by 3 %. The reason is that the annealing time increase from 1 h to 5 h, and the percentage of LAGB and KAM value decreases from 66.5 % to 52.3 % (Fig. 8) and from 0.83° to 0.47° (Fig. 9), respectively, indicating that the internal stress and the crystal defects are gradually reduced. Therefore, the electron scattering decreases and the EC of the samples is enhanced.

Fig. 12 exhibits the fracture morphologies of the samples annealed at different times, and it can be observed that the fracture dimple of the tensile samples increases gradually with the increase of annealing time, which further indicates that the plasticity of the material can be improved by the increase of annealing time.

Abbreviations

The following abbreviations and nomenclature are used in this manuscript:

Al	Aluminum
SEM	Scanning electron microscope
DC	Direct current
UTS	Ultimate tensile strength
EC	Electrical conductivity
EL	Elongation
YS	Yield strength
RE	Rare earths
EBSD	Electron backscattering diffraction
LAGB	Low-angle grain boundaries
IACS	International annealed copper standard
IACS	International Annealed Copper Standard
GB	Grain boundaries
IPF	Inverse pole figure
HAGB	High-angle grain boundaries
KAM	Kernel Average Misorientation
GND	Geometric necessary dislocation
SF	Schimid Factor

4. CONCLUSIONS

This paper presents an investigation into the effect of annealing temperature and time on the microstructure and properties of deformed Al wires. The principal conclusions are presented below.

1. As the annealing temperature is increased, the recrystallisation grain size and the SF value increase, while the percentage of LAGB and the KAM value decrease. Consequently, the internal stress and the crystal defects are reduced, resulting in the UTS being slightly decreased and the EL and EC increased. The samples with 50 % deformation begin to recrystallize annealed at 300 °C for 1h, and the recrystallization is completed after being annealed at 350 °C. The UTS decreases from 102.4 MPa to 77.7 MPa (decrease by 24 %), the EL increases by 74 % from 16.5 % to 28.7 %, and the EC increases by 3 % from 62.57 % IACS to 64.46 % IACS.

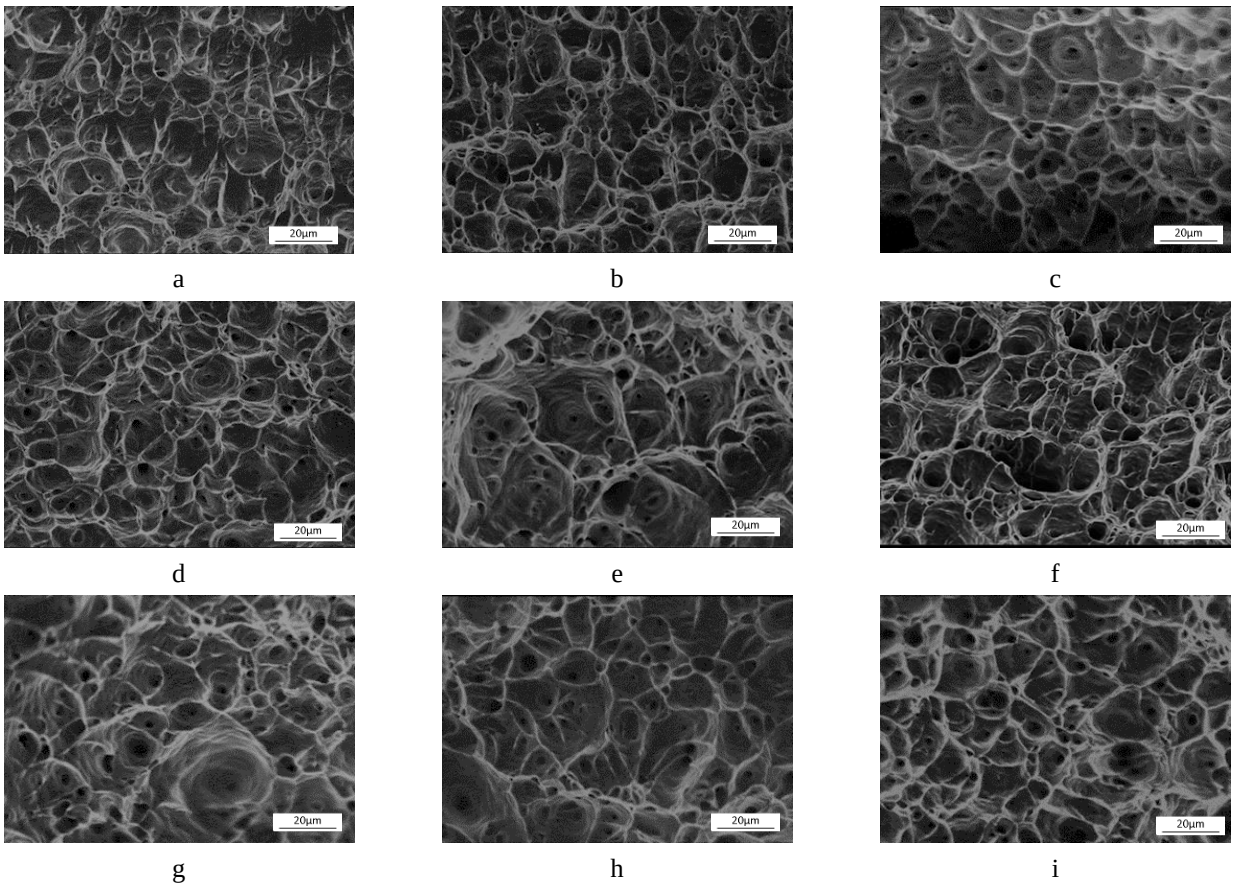

Fig. 12. Fracture morphologies of the samples annealed for different times: a – 1 h; b – 1.5 h; c – 2 h; d – 2.5 h; e – 3 h; f – 3.5 h; g – 4 h; h – 4.5 h; i – 5 h

2. Increasing the annealing time also increases the SF value of the sample, decreases the LAGB percentage and KAM value, and reduces the UTS is slightly decreased and the EL and EC are increased. When annealed for 1h at 315 ℃, the samples with 90 % deformation begin to recrystallize. After being annealed for 4.5 h, the recrystallization is completed. The UTS decreases from 108.69 MPa to 82.23 MPa (decrease by 24.3 %), the EL increases by 98 % from 14.16 % to 27.97 %, and the EC increases by 2.8 % from 63.06 % IACS to 64.82 % IACS.

Acknowledgments

This work was supported by Science and Technology Project from Guizhou Province (Grant No. [2023]267; [2022]031); The hundred-level innovative talents project of Guizhou Province (Grant No. GCC [2023]051).

REFERENCES

1. **Tsai, J.F., Shen, S.P., Lin, M.H.** Applying Fermatean Fuzzy Sets in Sustainable Development Assessment: A Case Study in the Wire and Cable Sector *Clean Technologies and Environmental Policy* 2024. https://doi.org/10.1007/s10098-024-02897-w
2. **Machado, M.R., Dutkiewicz, M.** Enhancing Broadband Vibration Suppression of a Cable Conductor Using Graded Metamaterials *Journal of the Brazilian Society of Mechanical Sciences and Engineering* 46 2024: pp. 190. https://doi.org/10.1007/s40430-024-04722-3
3. **Xie, Y., Zhao, Y., Bao, S., Wang, P., Huang, J., Wang, P., Liu, G., Hao, Y., Li, L.** Investigation on Cable Rejuvenation by Simulating Cable Operation *IEEE Access* 8 2020: pp. 6295 – 6303. https://doi.org/10.1109/ACCESS.2019.2963423
4. **Yu, F., Wang, S., Tang, K., Lin, Y., Wang, S., Zhang, Y.** Research Progress on the Fire Characteristics of Electric Cables and Wires *Fire* 7 (6) 2024: pp. 186. https://doi.org/10.3390/fire7060186
5. **Kaczorek-Chrobak, K., Fangrat, J.** Combustible Material Content vs. Fire Properties of Electric Cables *Energies* 13 (23) 2020: pp. 6172. https://doi.org/10.3390/en13236172
6. **Li, Y., Zhang, R., Yang, K., Qi, Y.** Research on an Equivalent Heat Source Model of the AC Arc in the Short Gap of a Copper-Core Cable and a Fire Risk Assessment Method *Sensors* 24 2024: pp. 1443. https://doi.org/10.3390/s24051443
7. **Hernandez-Robles, I.A., Gonzalez-Parada, A., Olivares-Galvan, J.C., Gonzalez-Ramirez, X.** Comparison of the Energy Potential of Copper and Superconducting Linear Electric Generators *IEEE Transactions on Applied Superconductivity* 29 2019: pp. 1 – 5. https://doi.org/10.1109/TASC.2018.2856840
8. **Wu, C.J., Sheng, Y.J., Tsao, H.K.** Copper Conductive Lines on Flexible Substrates Fabricated at Room Temperature *Journal of Materials Chemistry C* 4 2016: pp. 3274 – 3280). https://doi.org/10.1039/C6TC00234J

9. **Santana Martinez, G.A., Qian, W.L., Kabayama, L.K., Prisco, U.** Effect of Process Parameters in Copper-Wire Drawing *Metals* 10 2020: pp. 105. https://doi.org/10.3390/met10010105
10. **Georgantzia, E., Gkantou, M., Kamaris, G.S.** Al Alloys as Structural Material: A Review of Research *Engineering Structures* 227 2021: pp. 111372. https://doi.org/10.1016/j.engstruct.2020.111372
11. **Wang, Q., He, X., Deng, Y., Zhao, J., Guo, X.** Experimental Study of Grain Structures Evolution and Constitutive Model of Isothermal Deformed 2A14 Aluminum Alloy *Journal of Materials Research and Technology* 12 2021: pp. 2348 – 2367. https://doi.org/10.1016/j.jmrt.2021.04.025
12. **Okayasu, M., Ota, K., Takeuchi, S., Ohfuji, H., Shiraishi, T.** Influence of Microstructural Characteristics on Mechanical Properties of ADC12 Aluminum Alloy *Materials Science and Engineering: A* 592 2014: pp. 189 – 200. https://doi.org/10.1016/j.msea.2013.10.098
13. **Kim, C.S., Cho, K., Manjili, M.H., Nezafati, M.** Mechanical Performance of Particulate-Reinforced Al Metal-Matrix Composites (MMCs) and Al metal-matrix nano-composites (MMNCs) *Journal of Materials Science* 52 2017: pp. 13319 – 13349. https://doi.org/10.1007/s10853-017-1378-x
14. **Smyrak, B.** Analysis of the Quality of Aluminum Overhead Conductors after 30 Years of Operation *Engineering Failure Analysis* 154 2023: pp. 107600. https://doi.org/10.1016/j.engfailanal.2023.107600
15. **Hou, J.P., Li, R., Wang, Q., Yu, H.Y., Zhang, Z.J., Chen, Q.Y., Ma, H., Li, X.W., Zhang, Z.F.** Origin of Abnormal Strength-Electrical Conductivity Relation for an Al–Fe Alloy Wire *Materialia* 7 2019: pp. 100403. https://doi.org/10.1016/j.mtla.2019.100403
16. **Levin, A.A., Narykova, M.V., Lihachev, A.I., Kardashev, B.K., Kadomtsev, A.G., Brunkov, P.N., Panfilov, A.G., Prasolov, N.D., Sultanov, M.M., Kuryanov, V.N., Tyshkevich, V.N.** Modification of the Structural, Microstructural, and Elastoplastic Properties of Aluminum Wires after Operation *Metals* 11 2021: pp. 1955. https://doi.org/10.3390/met11121955
17. **Omrani, A., Dieng, L., Langlois, S., Van Dyke, P.** Friction Properties at the Contact Interfaces of Overhead Line Al Conductors *IEEE Transactions on Power Delivery* 37 2022: pp. 442 – 448. https://doi.org/10.1109/TPWRD.2021.3062704
18. **Jurkiewicz, B., Smyrak, B.** Studies on the Evolution of Fatigue Strength of Al Wires for Overhead Line Conductors *Materials* 17 2024: pp. 2537. https://doi.org/10.3390/ma17112537
19. **Pan, L., Liu, K., Breton, F., Grant Chen, X.** Effect of Fe on Microstructure and Properties of 8xxx Aluminum Conductor Alloys *Journal of Materials Engineering and Performance* 25 2016: pp. 5201 – 5208. https://doi.org/10.1007/s11665-016-2373-0
20. **Hou, J.P., Wang, Q., Zhang, Z.J., Tian, Y.Z., Wu, X.M., Yang, H.J., Li, X.W., Zhang, Z.F.** Nano-scale precipitates: The Key to High Strength and High Conductivity in Al Alloy Wire *Materials & Design* 132 2017: pp. 148 – 157. https://doi.org/10.1016/j.matdes.2017.06.062
21. **Luo, X.M., Song, Z.M., Li, M.L., Wang, Q., Zhang, G.P.** Microstructural Evolution and Service Performance of Cold-drawn Pure Aluminum Conductor Wires *Journal of Materials Science & Technology* 33 2017: pp. 1039 – 1043. https://doi.org/10.1016/j.jmst.2016.11.018
22. **Hou, J.P., Chen, Q.Y., Wang, Q., Yu, H.Y., Zhang, Z.J., Li, R., Li, X.W., Zhang, Z.F.** Effects of Annealing Treatment on the Microstructure Evolution and the Strength Degradation Behavior of the Commercially Pure Al Conductor *Materials Science and Engineering: A* 707 2017: pp. 511 – 517. https://doi.org/10.1016/j.msea.2017.09.075
23. **Zhao, Y., Li, L., Lu, Z., Teng, G., Liu, S., Hu, Z., He, A.** The Effect of Annealing Temperature on the Recrystallization and Mechanical Properties of Severe Plastic Deformed Commercial Pure Al During Ultra-Fast Annealing *Materials Research Express* 8 2021: pp. 046515. https://doi.org/10.1088/2053-1591/abf3e3
24. **Wang, G., Song, D., Zhou, Z., Liu, Y., Liang, N., Wu, Y., Ma, A., Jiang, J.** Developing High-Strength Ultrafine-Grained Pure Al Via Large-Pass ECAP and Post Cryo-Rolling *Journal of Materials Research and Technology* 15 2021: pp. 2419 – 2428. https://doi.org/10.1016/j.jmrt.2021.09.085
25. **Hou, J.P., Wang, Q., Yang, H.J., Wu, X.M., Li, C.H., Li, X.W., Zhang, Z.F.** Microstructure Evolution and Strengthening Mechanisms of Cold-Drawn Commercially Pure Aluminum Wire *Materials Science and Engineering: A* 639 2015: pp. 103 – 106. https://doi.org/10.1016/j.msea.2015.04.102
26. **Wang, M., Lv, H., Zhang, C., Li, M., Gao, H., Wang, J., Sun, B.** High Strength High Electrical Conductivity Ultrafine-Grained Al–Y Alloy Processed Via Cold Drawing *Materials Science and Engineering: A* 772 2020: pp. 138824. https://doi.org/10.1016/j.msea.2019.138824
27. **Hou, J.P., Li, R., Wang, Q., Yu, H.Y., Zhang, Z.J., Chen, Q.Y., Ma, H., Wu, X.M., Li, X.W., Zhang, Z.F.** Breaking the Trade-Off Relation of Strength and Electrical Conductivity in Pure Al Wire by Controlling Texture and Grain Boundary *Journal of Alloys and Compounds* 769 2018: pp. 96 – 109. https://doi.org/10.1016/j.jallcom.2018.07.358
28. **Hou, J.P., Li, R., Wang, Q., Yu, H.Y., Zhang, Z.J., Chen, Q.Y., Ma, H., Wu, X.M., Li, X.W., Zhang, Z.F.** Three Principles for Preparing Al Wire with High Strength and High Electrical Conductivity *Journal of Materials Science & Technology* 35 2019: pp. 742 – 751. https://doi.org/10.1016/j.jmst.2018.11.013
29. **Son, H.W., Lee, J.C., Cho, C.H., Hyun, S.K.** Effect of Mg Content on the Dislocation Characteristics and Discontinuous Dynamic Recrystallization during the Hot Deformation of Al-Mg alloy *Journal of Alloys and Compounds* 887 2021: pp. 161397. https://doi.org/10.1016/j.jallcom.2021.161397
30. **Paul, H.** Study of the Microtexture of Recrystallized Al *Microchimica Acta* 145 2004: pp. 153 – 158. https://doi.org/10.1007/s00604-003-0145-7
31. **Wang, Y., Ren, L., Dong, J., Cao, C.** Influence of Cold Rolled Deformation Degree and Heating Rates on Crystallite Dimension and Recrystallization Fraction of Aluminum Plates *Crystals* 11 2021: pp. 1428. https://doi.org/10.3390/cryst11111428
32. **Argon, A.S., Haasen, P.** A New Mechanism of Work Hardening in the Late Stages of Large Strain Plastic Flow in F.C.C. and Diamond Cubic Crystals *Acta Metallurgica et Materialia* 41 1993: pp. 3289 – 3306. https://doi.org/10.1016/0956-7151(93)90058-Z

33. **Mishin, O.V., Godfrey, A., Juul Jensen, D., Hansen, N.** Recovery and Recrystallization in Commercial Purity Aluminum Cold Rolled to an Ultrahigh Strain *Acta Materialia* 61 2013: pp. 5354 – 5364. https://doi.org/10.1016/j.actamat.2013.05.024
34. **Nasrollahnejad, M., Miresmaeili, R., Abdollah-Zadeh, A.** Prediction of Grain Size and Dislocation Density in the Cold Spraying Process Using a Dislocation-Based Model *Journal of Materials Research and Technology* 28 2024: pp. 244 – 254. https://doi.org/10.1016/j.jmrt.2023.11.213
35. **Zheng, Z., Prastiti, N.G., Balint, D.S., Dunne, F.P.E.** The Dislocation Configurational Energy Density in Discrete Dislocation Plasticity *Journal of the Mechanics and Physics of Solids* 129 2019: pp. 39 – 60. https://doi.org/10.1016/j.jmps.2019.04.015
36. **Xia, D., Chen, X., Huang, G., Jiang, B., Tang, A., Yang, H., Gavras, S., Huang, Y., Hort, N., Pan, F.** Calculation of Schmid Factor in Mg Alloys: Influence of Stress State *Scripta Materialia* 171 2019: pp. 31 – 35. https://doi.org/10.1016/j.scriptamat.2019.06.014
37. **Nan, X.L., Wang, H.Y., Zhang, L., Li, J.B., Jiang, Q.C.** Calculation of Schmid Factors in Magnesium: Analysis of Deformation Behaviors *Scripta Materialia* 67 2012: pp. 443 – 446. https://doi.org/10.1016/j.scriptamat.2012.05.042
38. **Ma, M., Wang, B., Liu, H., Yi, D., Shen, F., Zhai, T.** Investigation of Fatigue Crack Propagation Behavior of 5083 Aluminum Alloy under Various Stress Ratios: Role of Grain Boundary and Schmid Factor *Materials Science and Engineering: A* 773 2020: pp. 138871. https://doi.org/10.1016/j.msea.2019.138871
39. **Sadeghi-Nezhad, D., Mousavi Anijdan, S.H., Lee, H., Shin, W., Park, N., Nayyeri, M.J., Jafarian, H.R.** The Effect of Cold Rolling, Double Aging and Overaging Processes on the Tensile Property and Precipitation of AA2024 Alloy *Journal of Materials Research and Technology* 9 2020: pp. 15475 – 15485. https://doi.org/10.1016/j.jmrt.2020.11.005
40. **Hou, J.P., Li, R., Wang, Q., Yu, H.Y., Zhang, Z.J., Chen, Q.Y., Ma, H., Li, X.W., Zhang, Z.F.** Origin of Abnormal Strength-Electrical Conductivity Relation for an Al–Fe Alloy Wire *Materialia* 7 2019: pp. 100403. https://doi.org/10.1016/j.mtla.2019.100403
41. **Goli, F., Jamaati, R.** Effect of Strain Path during Cold Rolling on the Microstructure, Texture, and Mechanical Properties of AA2024 Aluminum Alloy *Materials Research Express* 6 2019: pp. 066514. https://doi.org/10.1088/2053-1591/ab0a1f